**Engineering and Technology Journal**
**Journal homepage:** https://etj.uotechnology.edu.iq

# Dynamic Response Analysis of the Rotor Using the Jeffcott Method and Performance Improvement Using Active Magnetic Bearing

**Karrar B. Tuaib*, Qasim A. Atiyah , Imad A. Abdulsahib**

Mechanical Engineering Dept., University of Technology-Iraq, Alsina'a street,10066 Baghdad, Iraq
*Corresponding author Email: me.19.20@grad.uotechnology.edu.iq

## HIGHLIGHTS

- Dealing with the Jeffcott method to change the parameters affecting the rotating shaft.
- The greater the current flowing through the AMB coil at an appropriate air gap distance, the greater the controllability of the rotating shaft.
- There is a significant reduction in the amplitude of vibrations when the active magnetic bearing is added.

## ARTICLE INFO

**Handling editor:** Sattar Aljabair

**Keywords:**

Vibrations
Rotating-Bearing System
Jeffcott method
Magnetic bearing
Active magnetic bearing (AMB)

## ABSTRACT

The most common component of mechanical systems today is rotating machines. In these systems, vibration is caused by rotating components. As a result, to decrease the amplitude of vibrations created by rotating equipment, it's required to understand the system's behavior. In this work, the problem of vibrations in conventional bearing systems and the effect of adding active magnetic bearings to rotating machines to reduce the amplitude of vibrations are discussed. In this paper, the vibrations in the rotary bearing system were studied theoretically and analytically using simulation programs to calculate the natural frequencies and parameters affecting the performance. In the theoretical part, the shaft of the rotating bearing was analyzed by the Jeffcott method depending on several parameters that were changed with the frequency value to observe the amplitude of the vibration in the shaft. An analytical aspect by simulation, a representative model of active magnetic bearings was built using the COMSOL 2020 program, The effect of adding these bearings on capacitance, vibration reduction, and frequency behavior was examined. SolidWorks 2018 software was used to analyze the magnetic field and its distribution in the magnetic bearing coil. The results indicate that when active magnetic bearings were introduced to the rotating bearing shafts, the vibration amplitude was reduced by approximately 60%. From this work, it can be concluded that the system becomes more stable when the active magnetic bearing is added to the rotating bearing shaft, giving it a more stable and firm nature.

## 1. Introduction

Vibrations in dynamic rotating machines are a common problem that can cause great damage to the system and cause loosening of the structure and collapse of equipment. Therefore, studying vibrations in shafts of rotating bearings is very important to analyze the cause of system failure and reduce its efficiency.

The analysis of the dynamics of rotary machines is known as rotor dynamics. Due to gyroscopic moments, cross-coupled system forces, and the possibility of whirling instability, rotor dynamics differs from structural vibration studies [1]. Rigid rotor systems with linear or nonlinear elastic bearings are used in various industrial applications, including aboard rocket engines, revolving equipment in power stations, and power transmission gear trains. However, vibration can cause inefficiency, malfunction, and even catastrophic failure in spinning systems. As a result, modeling and comprehending their nonlinear systems has been a popular research issue [2-4].

When the rotor's rotational speed is a part of its natural frequency, it can show undesired subcritical super-harmonic resonances [5]. Although vibration is a normal part of rotating machinery, it has the potential to diminish productivity [6,7].

Several authors have based their efforts over the last 40 years on researching the dynamical behaviors of rotors. Extensive reports on the dynamical behaviors of the cracked Jeffcott rotor system were published by Wauer [8] and Dimarogonas [9]. They discovered a variety of dynamical phenomena that could be used to confirm the location of cracks in rotating machinery. Sinou et al. [10] used an alternative frequency/time-domain approach to investigate the rotor dynamic response. They discovered that a change in the rotor system's dynamical characteristics close to half of the resonant speed indicates the



http://doi.org/10.30684/etj.2022.133607.1196
Received 18 April 2022; Accepted 17 June 2022; Available online 24 September 2022
2412-0758/University of Technology-Iraq, Baghdad, Iraq

presence of a shaft crack. Ref. [11] addressed the nonlinear dynamics of a rotor system with asymmetrical viscoelastic supports. Using the harmonic balance process, the authors investigated the effects of various device parameters such as crack width, disk position, and disc thickness. Hou et al. [12] examined a Jeffcott rotor device with Duffing style nonlinearity when simulating an aircraft rotor under maneuver loads. The localized bifurcations of the system at 1:2 and 1:3 super-harmonic resonance cases were analyzed using the multiple scales perturbation method, according to the researchers. The dynamical behavior of a horizontally assisted nonlinear Jeffcott rotor system was investigated in Ref. [13], using the multiple-scale perturbation approach in an analytical context. At primary resonance, the amplitude-phase modulating equations controlling the device's lateral vibrations are removed. In terms of the disc's rotating speed, disc eccentricity, and crack depth, periodic-motion bifurcation diagrams are produced. Haslam et al. [3] presented a novel method for studying the complicated rotor–stator interaction, which combines a Jeffcott rotor assisted by a comprehensive bearing model with the generalized harmonic balance process. The bearing induced a strongly non-linear reaction, resulting in major frequency changes with an increased excitement amplitude and a stable and unstable operating area.

In an active magnetic bearing system, time delays in the feedback loop are inevitable, particularly with digital technology control systems. Large-time delays destabilize steady-state solutions, while small-time delays have little effect on their qualitative conduct. Indeed, when time delays were assumed minor, researchers appeared to disregard them in their models [14-16].

Singh and Tiwari [17] examined the vibration properties of a cracked Jeffcott rotor with an offset disk under an active magnetic bearing (AMB), which was used to enhance the rotor's radial positioning. The harmonics of vibration displacement and AMB current were calculated using full-spectrum FFT. Saeed, et al. [18] presented a modified positive position feedback controller to regulate the lateral vibrations in a Jeffcott rotor system with cubic and nonlinear quadratic systems. The suggested controller can minimize the vibration magnitudes to near-zero at any rotating velocity. Finally, Yektanezhad, et al. [19] examined the primary resonance of an active magnetic bearing flexible rotor (AMBs). The influence of bearing variables on the device's dynamic range was studied, and it was discovered that only forward modes were stimulated close to the primary resonances.

In this paper, the Jeffcott method will be discussed and mathematically studied in three different cases to investigate the amplitude of vibrations in the rotating bearing shaft. First, the Jeffcott method will determine how changing some rotor parameters affects the results. Following that, COMSOL Multiphysics, the system's modeling method, and the process of adding an active magnetic bearing (AMB) to the rotor to minimize vibration magnitude will be discussed. Next, the vibration amplitude in the presence and absence of AMB will be compared. Consequently, SolidWorks will be highlighted, and its significance in coil analysis for Active Magnetic Bearings (AMB) will be underlined. Finally, each method's results are presented, which should be logically acceptable.

## 2. Material and Mathematical Analysis

### 2.1 Jeffcott method

Jeffcott [20] made one of the first attempts to model a basic rotor system more than a century earlier, consisting of a single rotor linked to the ground through a bearing. The rotor is believed to travel only in one direction, but this is enough to examine the rotor's disbalance reaction, and the resonance can be seen at such critical speeds. As a result, this model has proven to be a valuable testbed for new modeling and analysis techniques. Furthermore, because of its simplicity and ease of computation, the simple Jeffcott rotor has been. It continues to be widely used in the literature to research the effect of different bearing nonlinearities on a rotating device in an isolated manner [21]. Simple Jeffcott rotors will be covered in three ways: Jeffcott rotor one, when the rotor is installed on relatively rigid bearings, leading to "shaft situations", and the shaft is very flexible in comparison to the bearing and base supports; this is referred to as simply ‘flexible rotors’, as shown in Figure 1. The second case is Jeffcott rotor two, which is when the rotor is installed on very flexible bearings, leading to "bearing situations", and the shaft is far stiffer than the bearing and base supports; this is referred to as simple ‘stiff rotors’, as shown in Figure 2. The third case is Jeffcott rotor three, where the rotor is mounted on very flexible bearings, resulting in "shaft-bearing situations", and the shaft is very flexible. This is referred to as simple ‘very flexible rotor - bearings’, as shown in Figure 3.

#### 2.1.1 Case one

Taking into account the extremely rigid bearing support ‘flexible rotors’

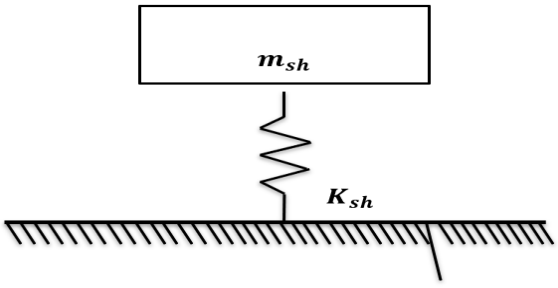


**Figure 1:** Simply supported beam with stiffness and mass of the shaft

$$I_i = \frac{\pi}{64} * d^4 \quad (1)$$

$$m_{sh} = \rho AL \quad (2)$$

$$K_{sh} = \frac{48EI_i}{L^3} \quad (3)$$

$$\omega_{nsh} = \sqrt{\frac{K_{sh}}{m_{sh}}} \quad (4)$$

### 2.1.2 Case two

The rotor shaft is substantially stiffer than bearing 'rigid rotors' since it is positioned on very flexible bearings.

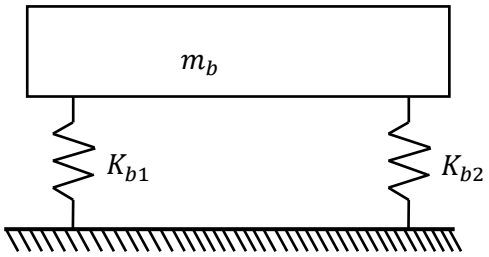


**Figure 2:** Simply Supported beam with Stiffness and mass of bearing

The stiffness of deep groove balls depends on the constants and equations mentioned in the source [22].

$$K_b = L_c * w^{1/3} \quad (5)$$

$$L_c = 531.6 * \left(\frac{2.4D_o + d_i}{D_o - d_i}\right)^{2/3} * \left(\frac{M_i}{m_i} c_i^1 + \frac{M_o}{m_o} c_o^1\right)^{-1} \quad (6)$$

$$\omega_b = \sqrt{\frac{k_b}{m_b}} \quad (7)$$

Where, $L_c$, $M_i/m_i$, $M_o/m_o$ , $c_i$, $c_o$ are constant, $w$ is applied load, and $D_o, d_i$ is outer and inner diameter, respectively.

### 2.1.3 Case three

The rotor shaft is flexible and positioned on very flexible bearings 'flexible rotor - bearing'.

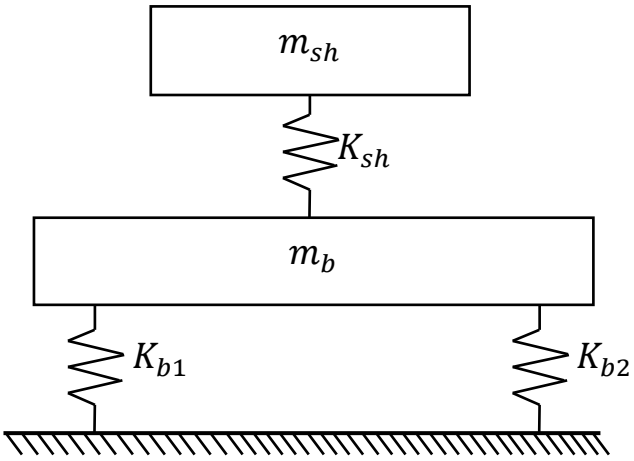


**Figure 3:** Simply Supported beam with Stiffness coefficient and mass equivalent

$$\frac{1}{K_{tot}} = \frac{1}{K_{sh}} + \frac{1}{2K_b} \tag{8}$$

$$\omega_{nt} = \sqrt{\frac{K_{tot}}{m_{sh}}} \tag{9}$$

## 2.2 COMSOL Multiphysics

The system is subjected to two time-dependent analyses to assess the impact of the active magnetic bearings on the system's total vibration. The initial analysis separates the active magnetic bearing from the device to acquire vibration levels in the device without any direct control (AMB). An AMB is triggered in the second analysis when the device's vibration is high due to resonance. The mechanism then responds to the AMB's increased control forces. The system's response to the AMB is directly compared to that of the structure without the AMB.

In this setup, an electric motor drives a rotor. In the simulation, the rotating velocity is gradually increased to replicate the system's starting. During startup, the system experiences critical velocities. As a result, the device produces high-amplitude vibrations. An electromagnetic bearing replaces a ball bearing to reduce vibrations during resonance in the rotor. Figure 4 shows a schematic representation of the device and an interior view of the electric motor to show the fan and rotor element inside and outside the electric motor.

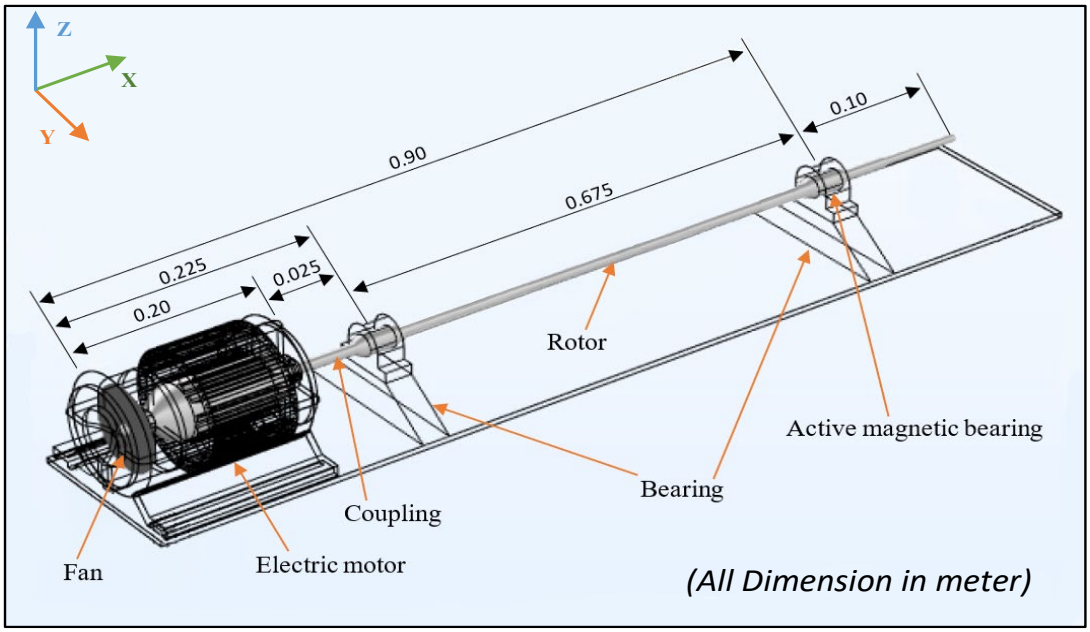


**Figure 4:** COMSOL System Structure Components

The motor and base are modeled using a Solid Mechanics interface. To emulate the rotor, a Beam Rotor graphical interface is used (both inside and outside the electric motor). The rotor inside the electric motor is connected to the rotor outside the motor via a strong connection. As a result, the genuine coupling is not represented; alternatively, the overall rotor is viewed as a single object. The disk functionality of the Beam Rotor graphical Interfaces is being used to replicate the fan within the power source. A lumped approximation represents both internal and external ball bearings with equal dynamic response values. The Active Magnetic Bearing features and functions of the Beam Rotor graphical interface provide the electromagnetic bearings. Table 1 shows the parameters of the rotor, while Table 2 shows the properties of the bearing. The type of bearing used in this work is a ball bearing, model UCP 204, made of cast iron.

## 2.3 Software Analysis

Solidworks software is used to analyze the magnetic fields in an active magnetic bearing coil based on the rotor measurements and dimensions mentioned in Table 1. In Figure (5a), the active magnetic bearing coil dimensions are shown where the magnetic flux directions within the magnetic bearing coil will be analyzed, as will be mentioned later in the results section. The basic structure of the active magnetic bearing is shown in Figure (5b). It consists of the radial stator, and the radial control coil. The stator core is made of AISI1010 steel. The stator is 8 magnetic poles symmetrically arranged in space, all of which are control shafts.

**Table 1:** Rotor's properties

| Parameter | Value |
|---|---|
| Young's modulus of the rotor (E) | 200 $(GPa)$ |
| Poisson's ratio of the rotor (ν) | 0.3 |
| The density of the rotor (ρ) | 7700 (Kg. $m^{-3}$) |
| Length of the rotor in the motor ($L_m$) | 0.20 (m) |
| Length of the rotor outside motor ($L_e$) | 0.80 (m) |
| Location of the first bearing in the motor | 0.035 (m) |
| Location of the second bearing in the motor | 0.14 (m) |
| Mass of the fan $(m_f)$ | 2.0 (kg) |
| Transverse moment of inertia of the fan $(I_{df})$ | 0.0079 (kg.$m^2$) |
| Polar moment of inertia of the fan $(I_{pf})$ | 0.0154 (kg. $m^2$) |

**Table 2:** Bearing properties

| Parameter | Value |
|---|---|
| Number of balls, $N_b$ | 8 |
| Ball diameter, $d_b$ | 8 (mm) |
| Pitch diameter, $d_P$ | 33.5 (mm) |
| Counter radius, inner race, $r_{in}$ | 12.75 (mm) |
| Counter radius, outer race, $r_{out}$ | 20.75 (mm) |
| Radial clearance, $c_r$ | 0.001 (mm) |
| Young modulus, inner race, $E_{in}$ | 200 (GPa) |
| Poisson's ratio, inner race, $v_{in}$ | 0.3 |
| AMB gap, $h$ | 2 mm |
| Bias current positive axis, $i_{bp}$ | 1 A |
| Bias current negative axis, $i_{bn}$ | 1 A |
| Maximum current, $i_{max}$ | 5 A |
| Proportional gain, $K_P$ | $2(i_{pn}^2 + i_{bn}^2)/((i_{bp} + i_{bn})h)$ |
| Integral gain, $K_i$ | $K_P$/0.001 |
| Derivative gain, $K_d$ | 0.005 $K_P$ |
| Force constant, $F_c$ | 20 |

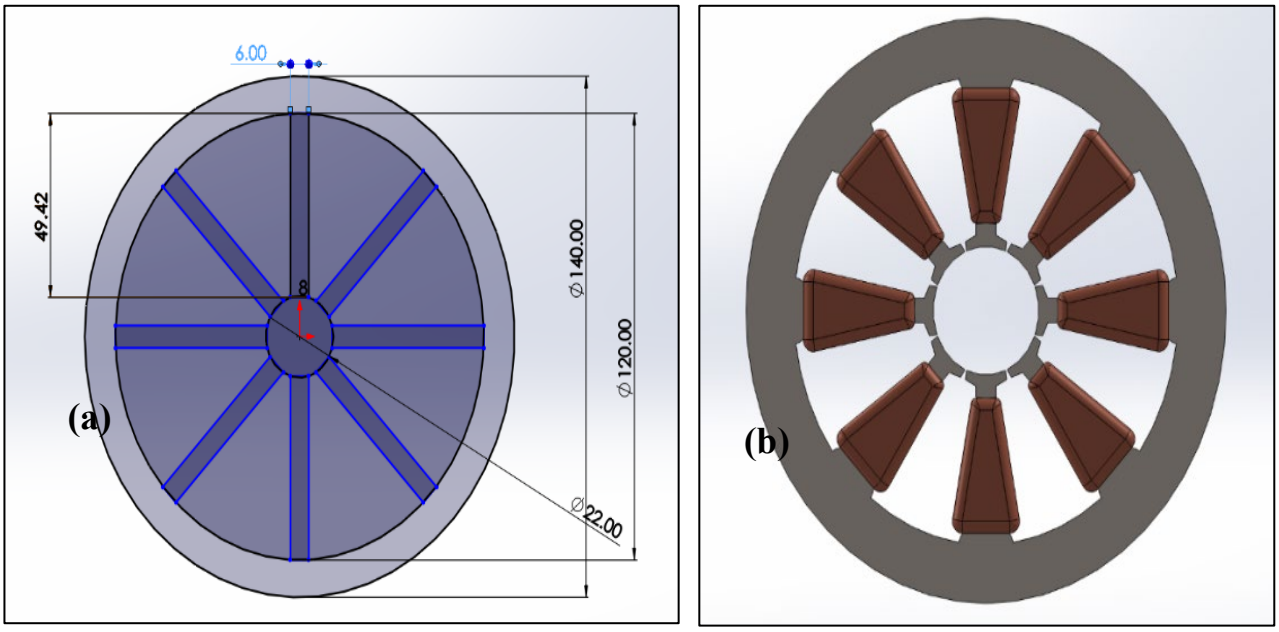


**Figure 5:** (a) Dimensions of the magnetic bearing coil, and (b) Coil of magnetic bearings with radial control

## 3. Results and Discussion

### 3.1 Analysis of shaft by the Jeffcott Method

Using Jeffcott's method and Equations 1 - 9, the various parameters are determined and presented in Table 3 based on the theoretical aspect, depending on the dimensions of the rotor shaft, whose specifications and dimensions are listed in Table 1. Table 3 shows the default and constant values when some parameters are changed in the Figures 6 - 11. The value of the natural frequency of the shaft in the first case, when the rotor is flexible, and the bearing is rigid, is almost half its value in the second case when the rotor is very rigid and the bearing is elastic. In the third case, when the rotor and bearing are resilient, it can be observed that the frequency value is approximately half its value in the first case. It is logical to note that the flexible bearings give a higher frequency value than the rigid bearings, as observed in the first and second cases. The same applies to the rotor. In the case of flexibility, its frequency is small compared to when the rotor is rigid, as in the three cases.

**Table 3:** Parameters of Uniform Shaft by Jeffcott Method

| Parameter | Value | Unit |
|---|---|---|
| $I_i$ | 7.8548E-09 | $(m^4)$ |
| $m_{sh}$ | 1.935 | $(Kg)$ |
| $k_{sh}$ | 147262.156 | $(N/m)$ |
| $f_{sh}$ | 43.904 | $(HZ)$ |
| $m_b$ | 0.11 | $(Kg)$ |
| $k_b$ | 47.23 | $(KN/m)$ |
| $f_b$ | 104.288 | $(HZ)$ |
| $k_{tot}$ | 57546.993 | $(N/m)$ |
| $f_{tot}$ | 27.445 | $(HZ)$ |

In the first case, a relationship is found between the natural frequency of the rotating shaft and some variables, as shown in Figures 6 - 8.

Figure 6 shows the relationship of the natural frequency of the rotating shaft in the first case (Equation 4) with the change of length with the constant of the other parameters found in Table 3. The relationship between the natural frequency of the shaft and the length is observed as an inverse relationship. The longer the shaft, the lower the value of the natural frequencies. Therefore, according to Equation 3, the increase in the length leads to a decrease in the stiffness of the shaft.

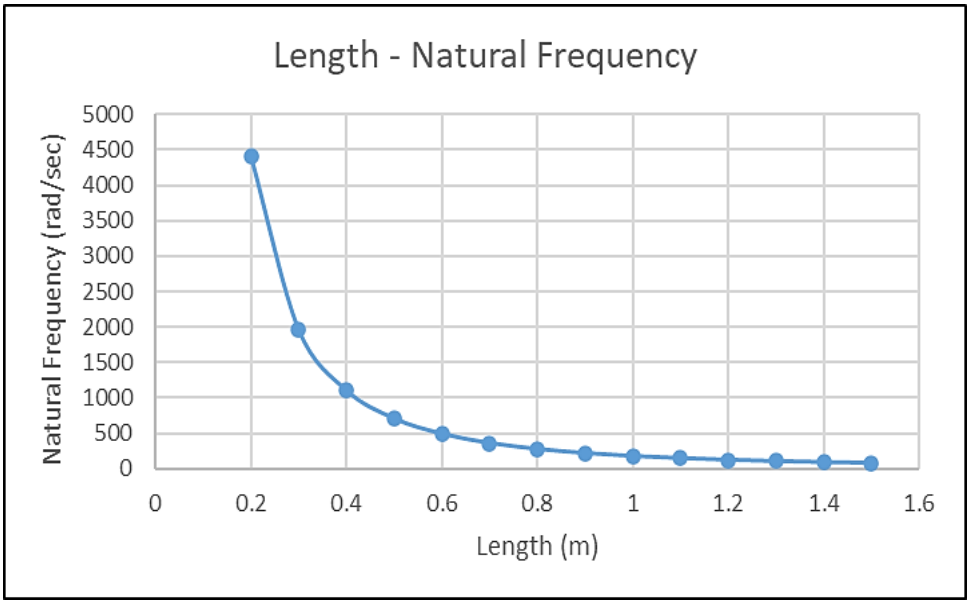


**Figure 6:** Relationship between the natural frequency of shaft with a length

Figure 7 manifests the relationship between the natural frequency of the shaft and the change in diameters in case one (Equations 1 – 4). The figure shows that the relationship between the diameter and the natural frequency is linear. The increase in the diameter leads to the increase in the natural frequencies.

Figure 8 evinces in case one (Equations 1 - 4) the variance of natural frequencies with the change in the elastic modulus ratio. As shown in the figure, the linear relationship between the modulus of elasticity and natural frequencies. The increase in the value of the elastic modulus leads to an increase in the stiffness of the shaft, and the frequencies value, as shown in Equation 3.

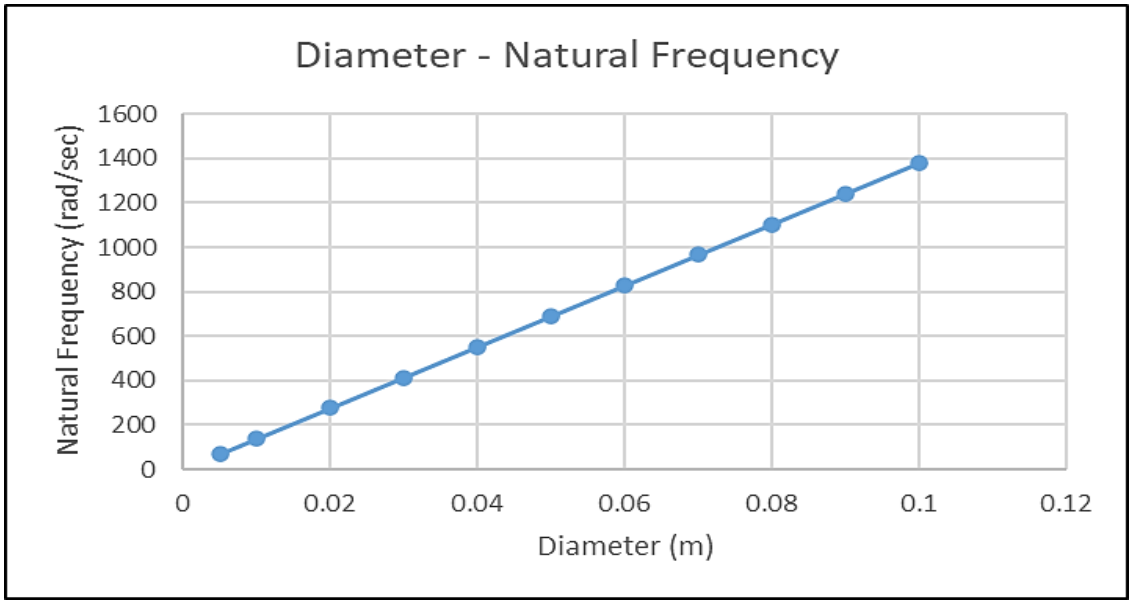


**Figure 7:** Relationship between the natural frequency of shaft with a diameter

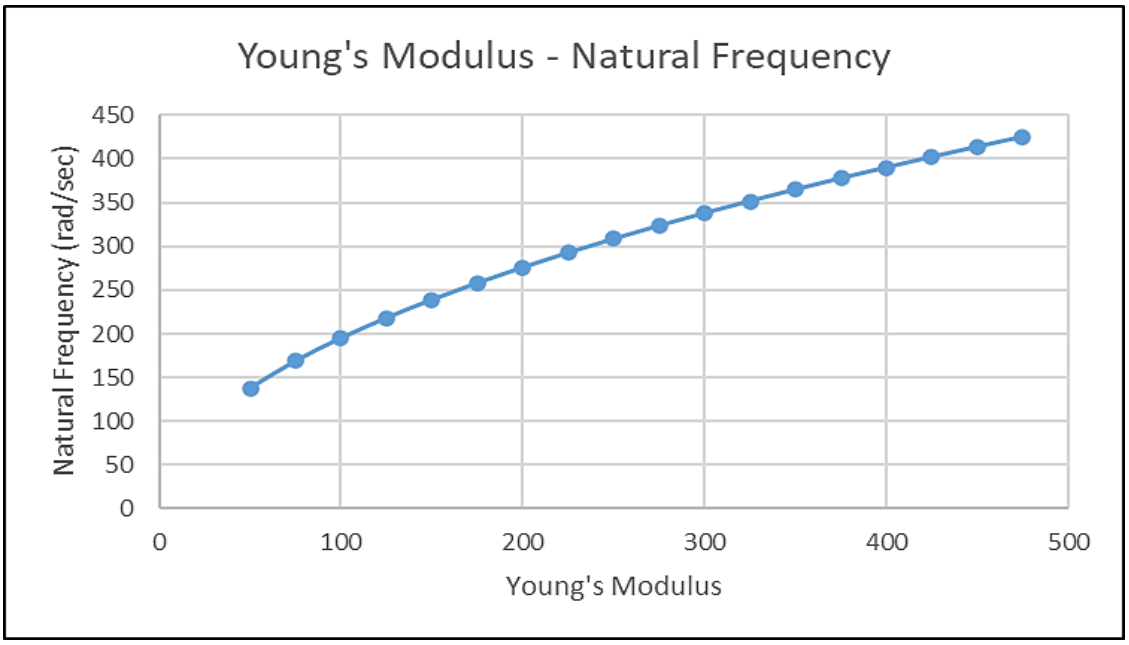


**Figure 8:** Variation of the natural frequency of shaft with Young's Modulus

In the second case, Figure 9 elucidates the variance relationship between the bearing stiffness with the natural frequencies of the bearing and the system's natural frequencies, depending on the different values of the bearing stiffness, with the constant of the other parameters in Table 3. By observing Figure 9, it can be observed that the natural frequency of the bearing increases with the increase in the stiffness of the bearing. Thise is because the natural frequency of the bearing is directly proportional to the stiffness of the bearing. As for the total natural frequency of the system, it increases slightly when the bearing stiffness increases, similar to the constant at a certain value. This is because the total stiffness depends on two parts of the stiffness, one of which is half of the bearing stiffness, as shown in Equation 8.

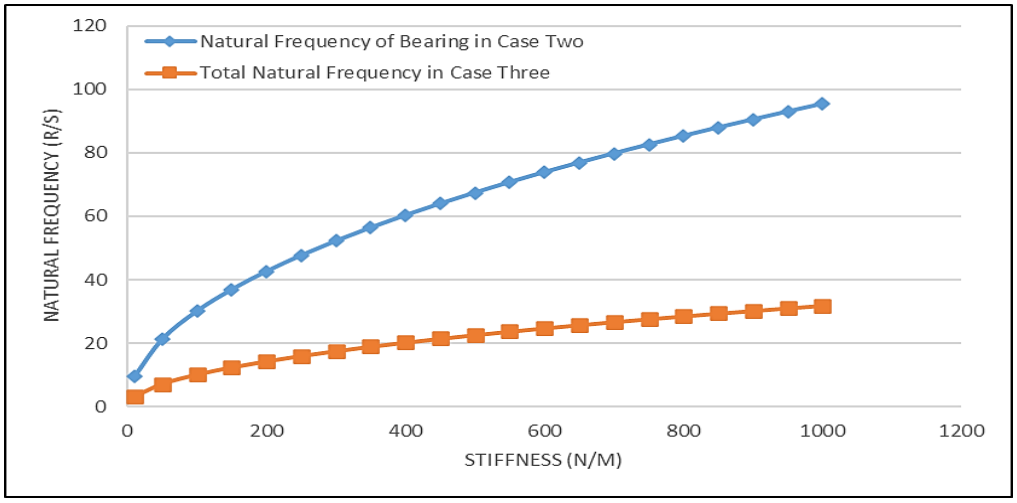


**Figure 9:** Relationship between the bearing stiffness with the natural frequency in a second and third case

In the third case (Equations 8, and 9), the density and shaft stiffness change with the total natural frequency of the system. Figure 10 shows the change of shaft stiffness with the system's natural frequency. It appears from the figure that the increase in stiffness leads to an increase in the total natural frequencies of the system, according to Equation 9. Finally, Figure 11 reveals the relationship between the change in masses and the system's natural frequencies. The figure shows that the increase in the weight of the shaft leads to a decrease in the system's natural frequency.

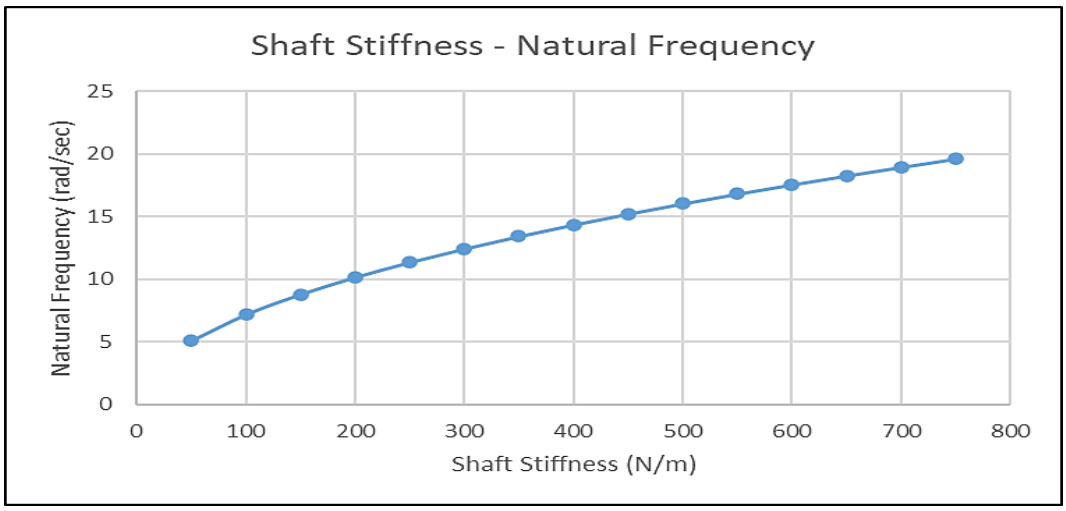


**Figure 10:** Relationship between the total natural frequency of the system with Shaft Stiffness in the third case

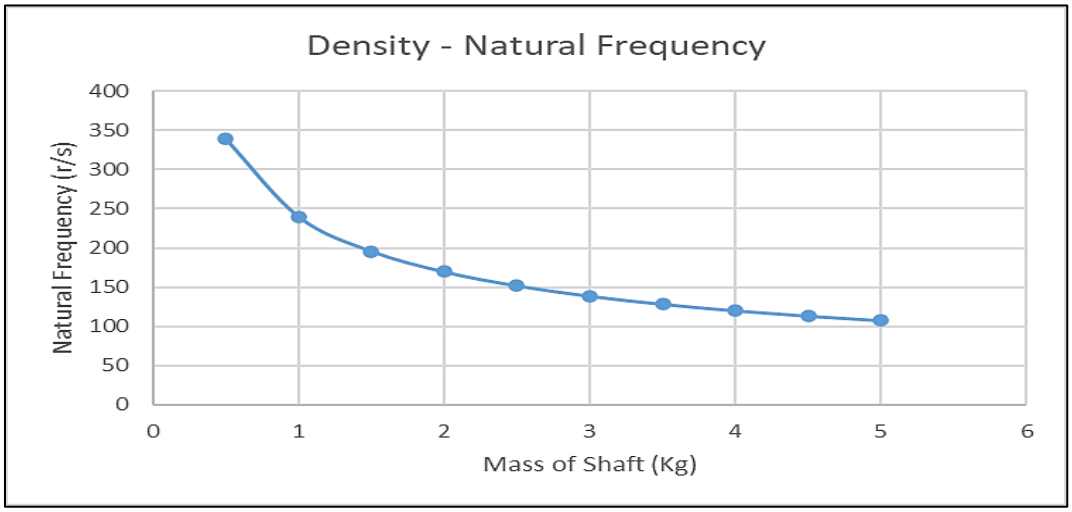


**Figure 11:** Relationship between the total natural frequency of the system with a density of shaft in the third case

### 3.2 Analysis of the shaft by magnetic bearing

The shaft displacement near the coupling and motor is shown in Figure 12. There is also a comparison of systems with and without AMB. The vibrations are minimized after the AMB is turned on, as illustrated in the diagram. As a result, AMB aids in preventing the propagation of instability throughout the shaft.

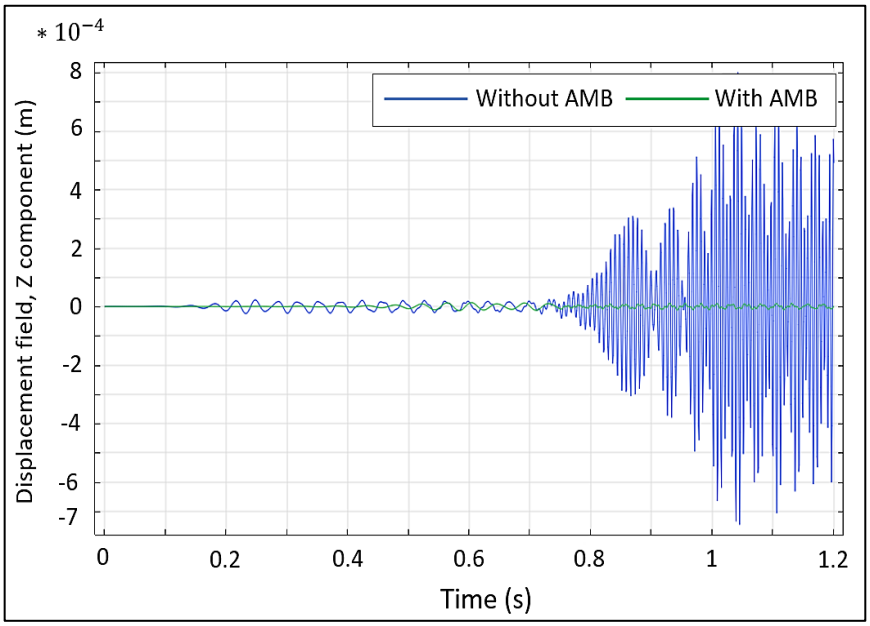


**Figure 12:** Vertical displacement of the shaft near the coupling with and without AMB

Figure 13 depicts the displacement of the rotating shaft. Where the comparison is performed in systems with and without AMB. After the AMB has switched on the system, shaft vibrations are regulated. As a result, AMB aids in the prevention of instability spreading throughout the shaft.

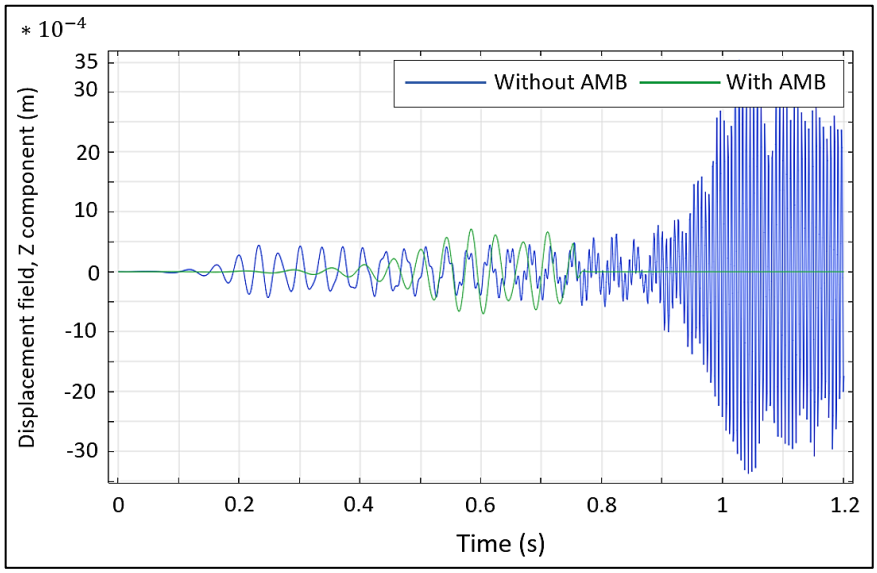


**Figure 13:** Vertical displacement of the shaft with and without active magnetic bearing

In Figures (12-13), because the shaft exhibits rotational speeds close to critical frequencies at the start of the system's operation, it will be subjected to large vibration amplitudes in the early moments. To eliminate them, an AMB system incorporates an again phase modifier (GPM) to build two closed loops that adaptively regulate the gain and phase of the synchronous control current. The GPM uses synchronous displacement and current signals derived from notch filters to compensate for phase lag caused by the power amplifier. As a result, the gain of the control current can be designed to compensate for the gain difference caused by the power amplifier and to control the rotation axis for the minimum vibration force and torque within the desired vibration displacement.

Variations in the amplitude of vibrations in the rotating apparatus can be observed with and without AMB. From the perspective of the previous figures, the system without the active magnetic bearing is observed to have relatively high vibration intensity. However, when the device's active magnetic bearing is installed, it will have a much lower vibration amplitude than in the first case. This can be demonstrated by converting the displacement data in Figure13 into acceleration data and analyzing it using the Fast Fourier Transform (FFT) method to obtain the frequency domain values. When there is no active magnetic bearing in the rotor, the frequency value reaches about 60 Hz and decreases to about 23 Hz when the active magnetic bearing is added to the system.

Figures 14–15 illustrate the contrast between conventional and magnetic bearings in the mode shapes, where Figure 14 shows the first mode shape, while Figures (15a) and (15b) show the second and third mode shapes, respectively. Based on this result, it was discovered that the magnitude of the vibrations was reduced by more than 60%, which is a great advantage. This indicates that the use of magnetic bearings provides very effective damping capabilities. Furthermore, in contrast to conventional bearings, magnetic bearings produce low amplitude vibrations due to their work with a small bandwidth of natural frequencies.

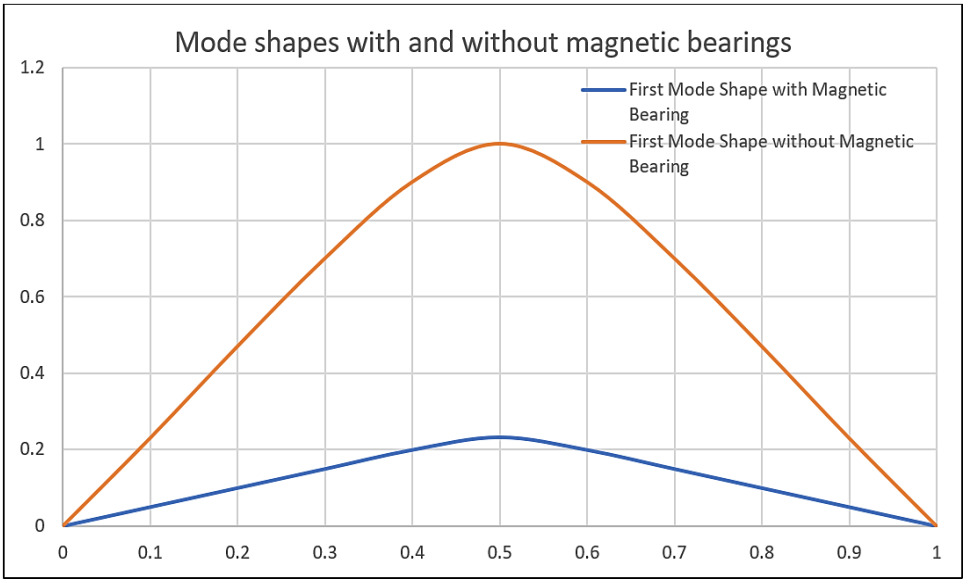


**Figure 14:** First mode shapes in the presence and absence of magnetic bearings

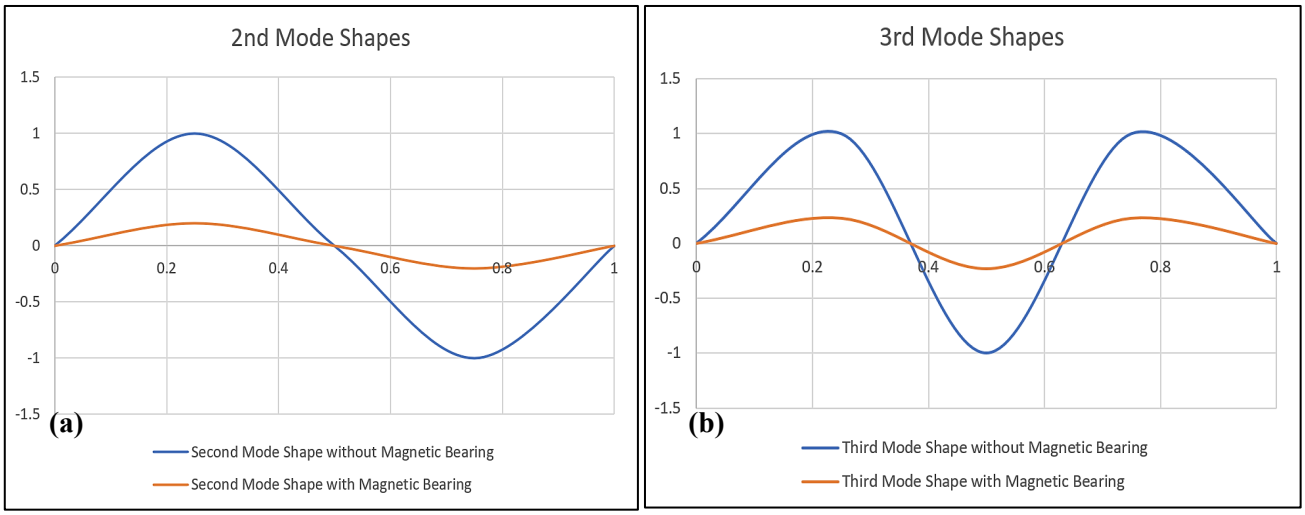


**Figure 15:** Second and third mode shapes in the presence and absence of magnetic bearings.

The clear benefit of magnetic bearings over standard bearings, as demonstrated in Figures 14-15, makes the study exciting and inspires researchers to analyze it thoroughly, explain its advantages, work on it, and fully incorporate it into the labor market industrial applications.

The finite element analysis (FEA) method is commonly employed in different engineering and electromagnetic disciplines. The rotor parameters listed in Table 1 can be used to create an FEA model for the proposed AMB. The magnetic field is

employed using the SolidWorks program to determine the magnetic field intensity and observe the flux density distribution of the proposed AMB, as shown in Figure (5b). The proposed AMB specifies the following mesh operations: The pole height in the stator is 49.42 mm, with a width of 6 mm; the length of the band areas and the air gap is 1 mm, and the length of the control windings is 3.5 mm. AISI 1010 steel is used for the stator and rotor.

Figure 16a shows the distribution of magnetic flux density, which shows the apparent distribution outside the magnet core when the rotor is in the center position without deflection, while Figure 16b shows the intensity of the magnetic field, which shows the internal distribution in the magnet core. Figure 17a depicts the coil's current density and Figure 17b shows the magnetic field intensity. Figure 18 depicts the magnetic bearing coil's directional flux density as well as the distribution strategy from the coil's outer circumference to its inner ring. This demonstrates that the field strength is stronger inside, improving the rotor's stability and control. Figure 19 depicts the same scenario as Figure 18 but with magnified magnetic flux density via the coils in those directions. As the stability near the center of the bearing grows, the flux will become more concentrated in this area.

Figures 16-19 show, the magnetic flux density and its distribution on the magnetic coil, where its highest values are at the poles near the rotating shaft. The closer the shaft is to the poles, the stronger the magnetic field attracts it. The lower the value of the air gap between the rotor and the bearing, the greater the magnetic force of attraction from the current. Thus, the stability of the rotor increases as the amplitude of vibrations and turbulence decreases, which means it can be controlled more easily.

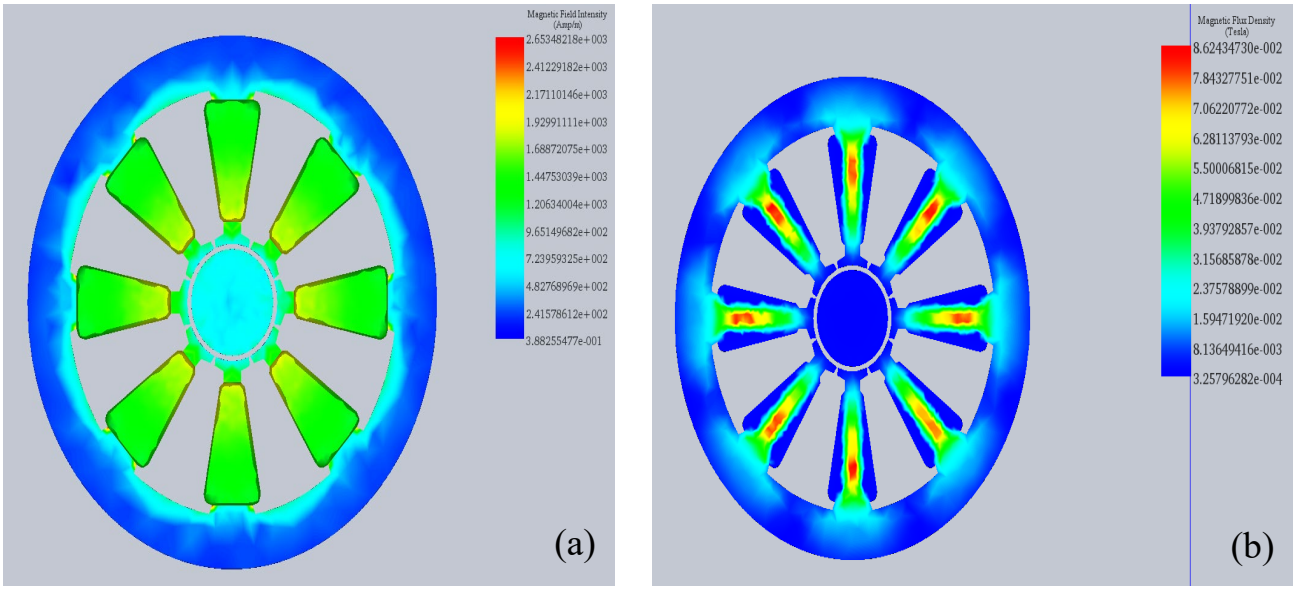


**Figure 16:** Distributed (a) magnetic field intensity and (b) magnetic flux density of coil AMB

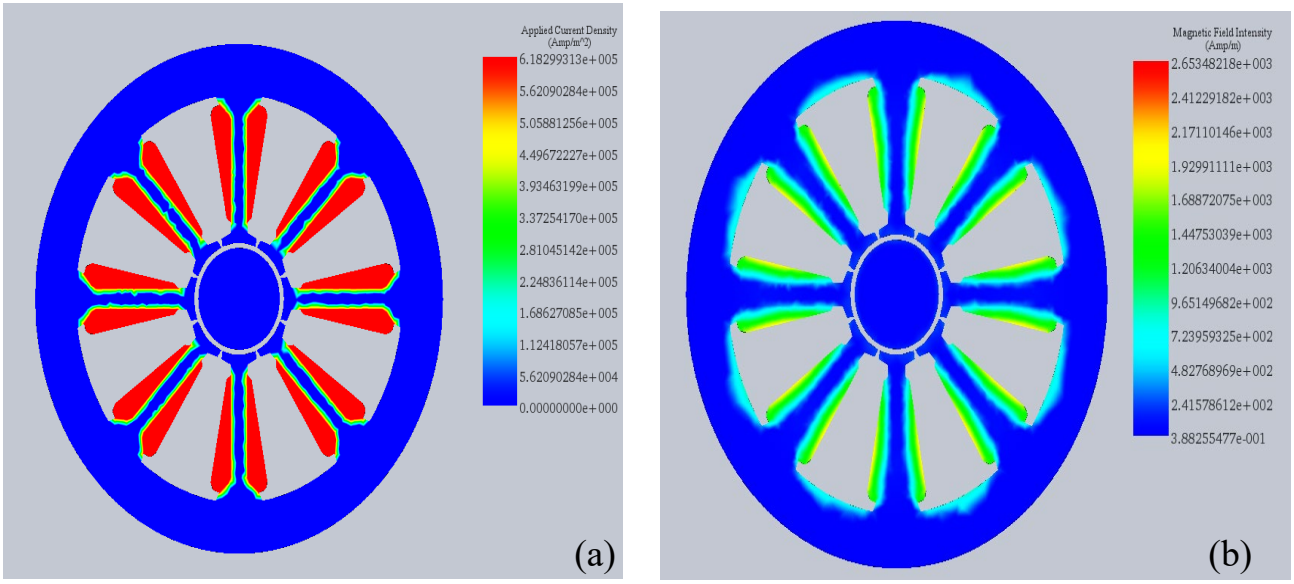


**Figure 17:** (a) Applied current density, (b) Magnetic field intensity of magnetic coil bearings

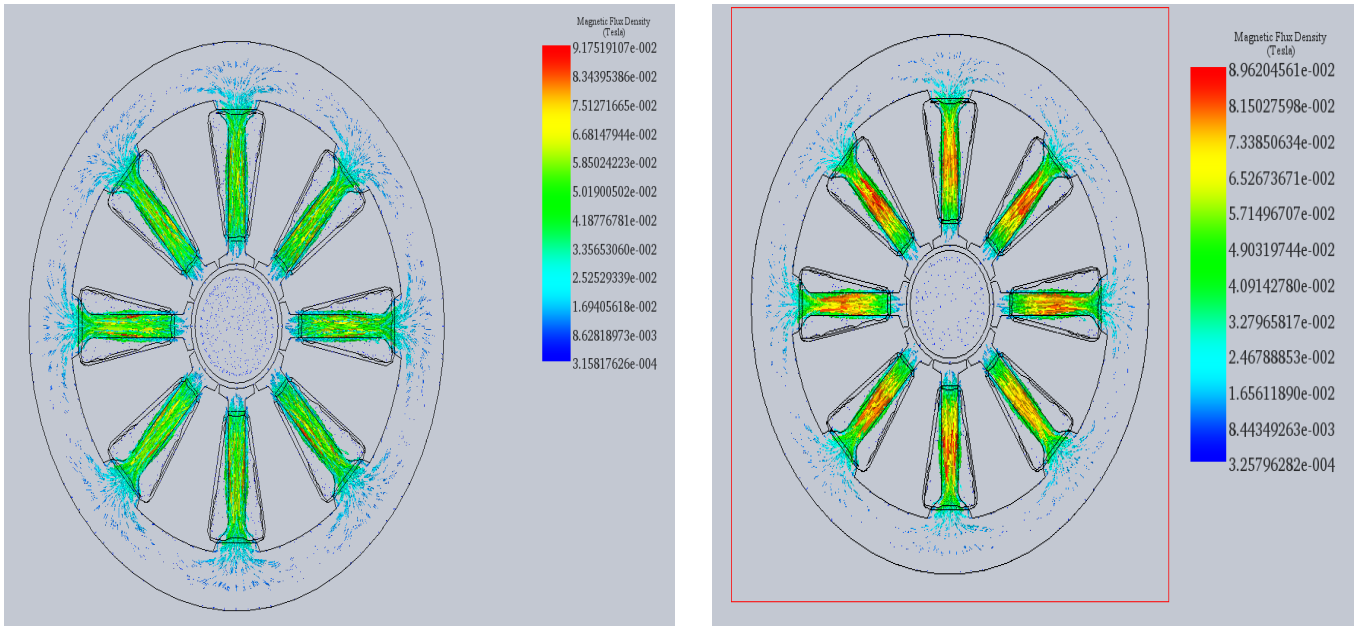


**Figure 18:** Directions flux density of magnetic bearing coil

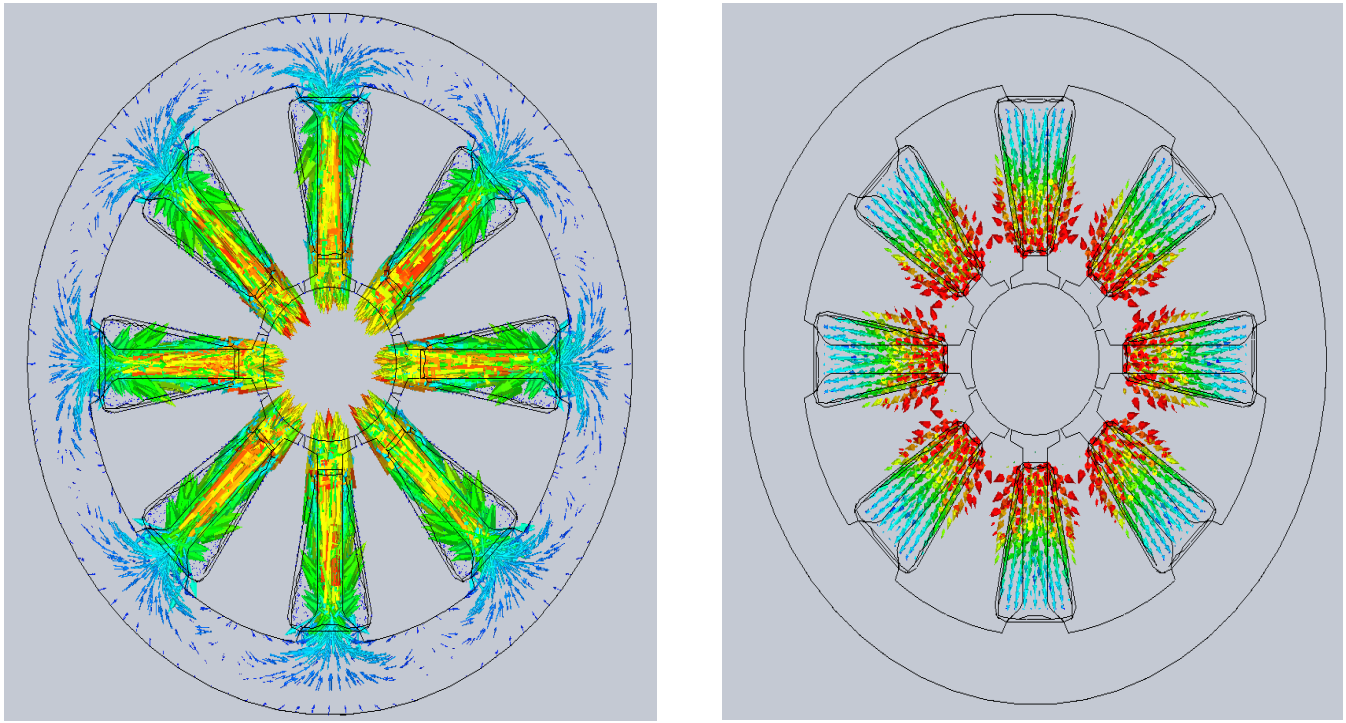

**Figure 19:** Magnetic flux density directions across coils

## 4. Conclusion

The Jeffcott method is described in this study for measuring the amplitude of vibrations in rotating shafts. The magnetic bearing was modeled and added to the system using the COMSOL program. The simulation was carried out in a representative manner. The results indicate that when the area cross-section of the rotating shaft increases, the value of the natural frequency also increases with it. The natural frequency increases with increasing the modulus of elasticity and the mass density of the shaft. Conversely, in length, the frequency decreases with increasing length.

According to this study, when magnetic bearings are used in rotating shafts, the intensity of shaft vibration is minimized. It was demonstrated that the magnitude of vibrations would be reduced by more than 60% in the first, second, and third mode shapes, which is a significant percentage that provides a perception of the damping loads imposed by magnetic bearings in mechanical devices and their significance in advanced technology. Furthermore, when the distance between the air gap is reduced, the magnetic field transmitted between the bearing and the rotor will increase with it, which leads to controlling the rotor and reducing the amplitude of vibrations in the system and giving it greater stability.

## 5. List of Symbol

| | | | |
|---|---|---|---|
| $A$ | Cross-sectional area ($m^2$) | $L$ | Length of the shaft (m) |
| $d$ | Diameter of shaft ($m$) | $L_c$ | Constant |
| $E$ | Young's modulus (Pa) | $m_b$ | Mass of bearing (Kg) |
| $I_i$ | Area moment of inertia for the uniform solid beam ($m^4$) | $m_{sh}$ | Mass of shaft |
| $K_b$ | Stiffness coefficient of bearing (N/m) | $\omega_b$ | The natural frequency of bearings (rad/s) |
| $K_{sh}$ | Stiffness coefficient of the shaft (N/m) | $\omega_{nsh}$ | The natural frequency of shaft (rad/s) |
| $K_{tot}$ | Stiffness coefficient equivalent (N/m) | $\omega_{nt}$ | Total natural frequency (rad/s) |
| | | $w$ | Applicable load (N) |
| | | $w$ | Applicable load (N) |

### Author contribution

All authors contributed equally to this work.

### Funding

This research received no specific grant from any funding agency in the public, commercial, or not-for-profit sectors.

### Data availability statement

The data that support the findings of this study are available on request from the corresponding author.

### Conflicts of interest

The authors declare that there is no conflict of interest.

### Reference

**[1]** J. M. Vance, F. Y. Zeidan, B. G. Murphy, Machinery vibration and rotordynamics, John Wiley & Sons, 2010.

**[2]** F. M. A. El-Saeidy, F. Sticher, Dynamics of a Rigid Rotor Linear/Nonlinear Bearings System Subject to Rotating Unbalance and Base Excitations, J. Vib. Control, 16 (2009) 403-438. https://doi.org/10.1177/1077546309103565

**[3]** A. H. Haslam, C. W. Schwingshackl, A. I. J. Rix, A parametric study of an unbalanced Jeffcott rotor supported by a rolling-element bearing, Nonlinear Dynamics, 99 (2020) 2571-2604. https://doi.org/10.1007/s11071-020-05470-4

**[4]** A. Khadersab, S. Shivakumar, Vibration analysis techniques for rotating machinery and its effect on bearing faults, Procedia Mfg., 20 (2018) 247-252. https://doi.org/10.1016/j.promfg.2018.02.036

**[5]** J. Heikkinen, B. Ghalamchi, J. Sopanen, A. Mikkola, Twice-Running-Speed Resonances of a Paper Machine Tube Roll Supported by Spherical Roller Bearings: Analysis and Comparison With Experiments, ASME 2014 International Design Engineering Technical Conferences and Computers and Information in Engineering Conference, American Society of Mechanical Engineers Digital Collection, 2014. https://doi.org/10.1115/DETC2014-34220

**[6]** R. V. Daniel, S. A. Siddhappa, S. B. Gajanan, S. V. Philip, P. S. Paul, Effect of Bearings on Vibration in Rotating Machinery, IOP Conference Series Mater. Sci. Eng., Karunya University, Coimbatore 641114, Tamil Nadu, India.,225 (2017). https://doi.org/10.1088/1757-899X/225/1/012264

**[7]** G. Chandrashekar, W. Raj, C. Godwin, P. S. Paul, Study On The Influence Of Shaft Material On Vibration In Rotating Machinery, Mater. Today Proc., 5 (2018) 12071-12076. https://doi.org/10.1016/j.matpr.2018.02.182

**[8]** J. r. Wauer, On the dynamics of cracked rotors: a literature survey, Appl. Mech. Rev., 43 (1990) 13-17. https://doi.org/10.1115/1.3119157

**[9]** A. D. Dimarogonas, Vibration of cracked structures: A state of the art review, Eng. Fract. Mech., 55 (1996) 831-857. https://doi.org/10.1016/0013-7944(94)00175-8

**[10]** J. J. Sinou, A. W. Lees, The influence of cracks in rotating shafts, J. Sound Vib., 285 (2005) 1015-1037. https://doi.org/10.1016/j.jsv.2004.09.008

**[11]** L. Dai, C. Chen, Dynamic stability analysis of a cracked nonlinear rotor system subjected to periodic excitations in machining, J. Vib. Control, 13 (2007) 537-556. https://doi.org/10.1177/1077546307074242

**[12]** L. Hou, Y. Chen, Z. Lu, Z. Li, Bifurcation analysis for 2:1 and 3:1 super-harmonic resonances of an aircraft cracked rotor system due to maneuver load, Nonlinear Dynamics, 81 (2015) 531-547. https://doi.org/10.1007/s11071-015-2009-1

**[13]** N. A. Saeed, M. Eissa, Bifurcations of periodic motion of a horizontally supported nonlinear Jeffcott rotor system having transversely cracked shaft, Int. J. Non-Linear Mech., 101 (2018) 113-130. https://doi.org/10.1016/j.ijnonlinmec.2018.02.005

**[14]** L. Virgin, T. Walsh, J. Knight, Nonlinear behavior of a magnetic bearing system, J. Eng. Gas Turbines Power, 117 (1995) 52-588. https://doi.org/10.1115/1.2814135

**[15]** J. Ji, C. Hansen, Non-linear oscillations of a rotor in active magnetic bearings, J. Sound Vib., 240 (2001) 599-612. https://doi.org/10.1006/jsvi.2000.3257

**[16]** G. Genta, S. Carabelli, Noncolocation effects on rigid body rotordynamics of rotors on AMB, Proceedings of the seventh international symposium on magnetic bearings, ETH Zurich, (2000) 63-68.

**[17]** S. Singh, R. Tiwari, Model-Based Switching-Crack Identification in a Jeffcott Rotor With an Offset Disk Integrated With an Active Magnetic Bearing, J. Dyn. Syst. Meas. Contr., 138 (2016). https://doi.org/10.1115/1.4032292

**[18]** N. Saeed, M. Kamel, Active magnetic bearing-based tuned controller to suppress lateral vibrations of a nonlinear Jeffcott rotor system, Nonlinear Dynamics, 90 (2017) 457-478. https://doi.org/10.1007/s11071-017-3675-y

**[19]** A. Yektanezhad, S. Hosseini, H. Tourajizadeh, M. Zamanian, Vibration analysis of flexible shafts with active magnetic bearings, Iran. J. Sci. Technol. Trans. Mech. Eng., 44 (2018) 403-414. https://doi.org/10.1007/s40997-018-0263-9

**[20]** H. H. Jeffcott, The lateral vibration of loaded shafts in the neighbourhood of a whirling speed.—The effect of want of balance, Lond.Edinb.Dubl.Phil. Mag. J. Sci., 37 (2009) 304-314. https://doi.org/10.1080/14786440308635889

**[21]** H. Cao, L. Niu, S. Xi, and X. Chen, Mechanical model development of rolling bearing-rotor systems: A review, Mech. Syst. Signal Process., 102 (2018) 37-58. https://doi.org/10.1016/j.ymssp.2017.09.023

**[22]** H. El-Sayed, Stiffness of deep-groove ball bearings, Wear, 63 (1980) 89-94. https://doi.org/10.1016/0043-1648(80)90075-7